Nonlinear Optics in Relativistic Plasmas and Laser Wake Field Acceleration of Electrons

D. Umstadter, S.-Y. Chen, A. Maksimchuk, G. Mourou, R. Wagner

When a terawatt-peak-power laser beam is focused into a gas jet, an electron plasma wave, driven by forward Raman scattering, is observed to accelerate a naturally collimated beam of electrons to relativistic energies (up to 10^9 total electrons, with an energy distribution maximizing at 2 megaelectron volts, a transverse emittance as low as 1 millimeter-milliradian, and a field gradient of up to 2 gigaelectron volts per centimeter). Electron acceleration and the appearance of high-frequency modulations in the transmitted light spectrum were both found to have sharp thresholds in laser power and plasma density. A hole in the center of the electron beam may indicate that plasma electrons were expelled radially.

High-intensity laser-plasma interactions are of much current interest because of their relevance to advanced concepts for accelerators, radiation sources, astrophysics, and inertial confinement thermonuclear fusion. When a terawatt-peak-power laser is focused to high intensity into a gas, a plasma is created by tunneling ionization, and the free electrons begin to quiver at velocities close to the speed of light (c) in the laser's transverse oscillating electromagnetic field. The laser light phase velocity v_ϕ depends on the index of refraction $v_\phi = c/n$, where the latter is given by

$$n = [1 - (\omega_p/\omega)^2]^{1/2} \quad (1)$$

where ω is the laser frequency and the plasma frequency is given by

$$\omega_p = (4\pi n_e e^2/\gamma m_0)^{1/2} \quad (2)$$

where e is the electron charge, m_0 is the electron rest mass, and n_e is the plasma electron density. The relativistic factor γ associated with the motion perpendicular to the direction of laser propagation depends on the laser field through the electron quiver velocity v_{os}, $\gamma = [1 + a^2]^{1/2}$, where $a = \gamma v_{os}/c = eE/m_0\omega c = 8.5 \times 10^{-10}\lambda I^{1/2}$ is the normalized vector potential, E is the laser electric field, $I = cE^2/8\pi$ (W cm^{-2}) is the laser intensity, and λ (μm) is the wavelength. Because local variations in the laser intensity will modify the index, this will in turn locally modify the laser intensity, and so on. Hence, novel effects in a new regime of nonlinear optics will arise.

The index can be modified by the laser directly through variations in γ. For example, a phenomenon called relativistic self-phase modulation accompanies rapid temporal changes in γ, which may both broaden and modulate the transmitted light spectrum (*1*). Another example is self-focusing, which can occur because the laser intensity varies with the radius. The plasma then acts as a positive lens, focusing the laser to a smaller spot size and increasing the peak laser intensity. It occurs at a critical power (*1*) given approximately by $P_c = 17(\omega/\omega_{p0})^2$ GW $= 17 n_c/n_e$ GW, where n_c is the critical density (at which ω_p equals ω).

Variations in the plasma density will also modify the index. For instance, the gigabar pressure that results from electron quiver motion in the field of a self-focused laser can create an evacuated channel in a process called electron cavitation (*2*). An electron density minimum on axis will also produce a radially dependent index of refraction and thus is predicted to focus and guide the laser pulse (*3*–*5*). Photoionization has the opposite effect, defocusing the laser because it produces a higher electron density on axis. The pressure is the time-averaged quiver energy density, $p = n_e(1/2)\gamma m_0\langle v_{os}^2\rangle$. Pressure gradients will push electrons to regions of lower intensity through the ponderomotive force $F = \nabla p \propto \nabla(n_e I\lambda^2)$. If the radial force becomes large enough for a long enough period of time, the electrons that get pushed out first will eventually drag the ions from the channel.

Laser pressure—combined with ion inertia, which provides an electrostatic restoring force—can also drive a high-amplitude electron plasma wave (EPW). By this process, some of the laser energy is converted to a longitudinal electrostatic laser wake field, propagating at nearly the speed of light, which can continuously accelerate electrons in the direction of laser propagation to gigaelectron volt energies in a distance as short as a centimeter. A comparable electron energy would require acceleration over a distance of tens of meters in a conventional radio-frequency linear accelerator. Thus, laser wake fields combined with the recent large reduction in the size of high-power lasers (*6*) can dramatically reduce the size of electron accelerators (*7*).

If the laser pulse width τ is much greater than a plasma period ($\tau \gg 2\pi/\omega_p$), the resulting local density changes will have time to provide feedback on the light pulse (*8*–*14*). For example, in the case of the stimulated Raman forward scattering (RFS) instability, modulations in the index of refraction break the pulse into a sequence of shorter pulses with a periodicity equal to a plasma period, which "resonantly" drives the EPW to high amplitude. The RFS instability in one dimension, in the direct forward direction, is predicted to grow exponentially with a growth rate given by (*13*)

$$g(z,\tau) = [8(P/P_c)(n_c/n_e)(z/z_R)(\omega\tau)/(1 + a^2/2)]^{1/2} \quad (3)$$

where z/z_R is the laser propagation length normalized to the Rayleigh (vacuum diffraction) length and P/P_c is the laser power over the critical power. Raman backscatter and sidescatter both have higher growth rates (*15*). In two dimensions, RFS can be enhanced by relativistic self-focusing (*9*, *10*, *12*). Theory (*12*) predicts that in this case envelope self-modulation will occur at a power threshold of $P_c/2$.

Normally, electrons participating in the EPW oscillate about a fixed oscillation center. However, at sufficiently high ampli-

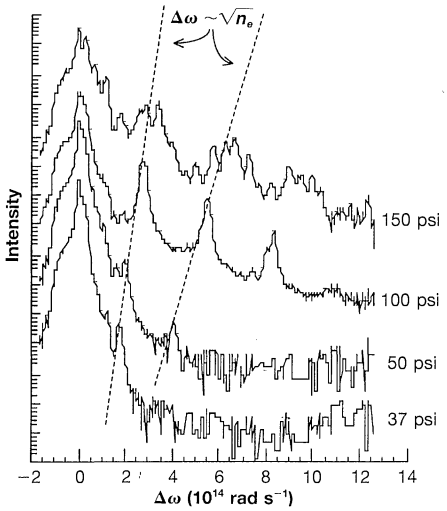

Fig. 1. Spectrum of RFS light as a function of backing pressure (electron density) for fixed laser power (6 TW). The curves are corrected for spectrometer-detector response and plotted on a logarithmic scale but are offset from each other to prevent overlap. Intensity is plotted on a log scale of arbitrary units.

Center for Ultrafast Optical Science, University of Michigan, Ann Arbor, MI 48109, USA.

tude, the EPW will trap electrons from the background plasma, a phenomenon often called wavebreaking. The maximum axial electric field of a relativistic plasma wave, as predicted by one-dimensional (1D) cold fluid theory, is the "wavebreaking" field (*16*), $E_{WB} = E_0\sqrt{2(\gamma_p - 1)}$, where E_0 (V cm^{-1}) = $(m_e c\omega_p/c) \simeq 0.96 n_e^{1/2}$ (cm^{-3}). This wavebreaking field will tend to decrease with finite temperature. Once trapped, the electrons become in phase with the electrostatic field of the EPW and can be continuously accelerated by it, damping the wave in the process.

We report here detailed experimental measurements of the dynamics of these interactions. In particular, we demonstrate acceleration of a naturally collimated beam of megaelectron volt electrons and determine its transverse emittance. RFS satellites begin to appear at a laser power of $P_c/2$, indicating that relativistic self-focusing may be occurring. At higher power, electron acceleration occurs with a sharp threshold, $(3/2)P_c$, along with the onset of broadening and high-frequency modulations in the transmitted light spectra. Under certain circumstances, a lower beam emittance and evidence for electron cavitation were both observed. These observations compare well with recent theoretical analysis and numerical simulations.

A high-power glass laser with a wavelength of 1.05 μm was focused into a jet of either He or Ar gas. The laser has a pulse duration (τ) of 400 fs ($\omega\tau$ = 716) and an energy of up to 3 J, corresponding to a peak power of 7.5 TW. When the laser was focused in a vacuum with an f/4 off-axis parabolic mirror, an intensity of up to 6.2×10^{18} W/cm^2 (a = 2.2) could be reached. An underdense plasma was created when the gas from a supersonic pulsed valve was multiphoton ionized by the foot of the laser pulse. The gas jet neutral density profile was characterized by use of laser-induced fluorescence. At the position in the jet downstream from the nozzle where the interaction takes place, the peak neutral density was 2.5×10^{20} cm^{-3}, with a sharp (200 μm) gradient and a flat-top width of 500 μm at a backing pressure of 350 psi (where 1 psi = 6.9 kPa). The neutral density was found to increase linearly with backing pressure. Helium was used for most of the experiments because it has fewer ionization stages, which simplifies the interpretation of the results.

The existence of a large-amplitude EPW was inferred from the presence of high-order satellites in the RFS spectra (*17*), obtained with a prism spectrometer with resolution $\lambda/\Delta\lambda$ = 600 at λ = 1.053 μm. In RFS spectra from He obtained at different values for the density for fixed laser power (6 TW) (Fig. 1), the frequency separation between satellites, given by the plasma-wave frequency ω_p, increases with the square root of the density, as expected from Eq. 2. The maximum electron density was 2.3×10^{19} cm^{-3} (corresponding to n_e/n_c = 0.02 and P_c = 730 GW), which was achieved when the laser was focused on the edge of the jet. This was apparently due to refraction caused by ionization defocusing, even in a He gas jet with a sharp gradient (*18*). That refraction is supported by other observations. Higher backing pressure did not increase n_e, the fundamental frequency was shifted toward a higher frequency in Figs. 1 and 2, and the transmitted laser beam has a large divergence angle. At these densities, the wave is close to the 2D limit, because the plasma wavelength ($2\pi c/\omega_p \sim 7$ μm) is only half the plasma wave transverse dimension ($2r \sim 17$ μm), which is assumed to be equal to the laser spot size (at $1/e^2$).

RFS spectra from He were obtained at different values of the laser power for a fixed electron density, 2.3×10^{19} cm^{-3} (Fig. 2). The first anti-Stokes satellite appears at P = 350 GW, which corresponds to $P_c/2$, precisely as predicted by theory (*12*). This indicates a possible role for relativistic self-focusing. The number and amplitude of the Raman satellites increase with increasing density and power as predicted by Eq. 3. The relative amplitude of the satellites can be used to determine the EPW amplitude (*19*, *20*), which is found to range from $\tilde{n}/n_e \sim 8$ to 40% (or $E_z \sim 0.5$ to 2 GeV cm^{-1}), corresponding to changing the power from 0.8 TW to 6.7 TW. A recent 2D particle-in-cell (PIC) code simulation (*21*), with parameters similar to our own (except τ = 600 fs with a propagation distance of 1 mm), predicts that the EPW will grow to $\tilde{n}/n_e \sim 40\%$ on the rising edge of the laser pulse, undergo wavebreaking, and then do the same on the falling edge.

At 1 TW, we observed a broadening of, and higher frequency modulations on, both the fundamental and the satellites. Similar modulations and broadening can be obtained numerically (*19*) by simulating relativistic self-phase modulation or temporal interference between light scattered from different EPWs during the rising and falling edges of the laser pulse.

As shown in Fig. 3, the electron energy distribution is measured with a magnetic spectrometer. First, the electrons are collimated with an aperture, then their momenta are dispersed with a permanent dipole magnet, and lastly they are detected with a scintillator screen imaged to a charge-coupled device (CCD) camera. The number of accelerated electrons was maximized at an energy of 2 MeV and fell exponentially with increasing energy with a width at the $1/e$ point of 1.6 MeV. The low-energy cutoff (near 1.7 MeV) in Fig. 3 should be noted. The energy distribution was independent of angle with respect to the laser axis.

Quantitative information on the number of electrons accelerated in the forward

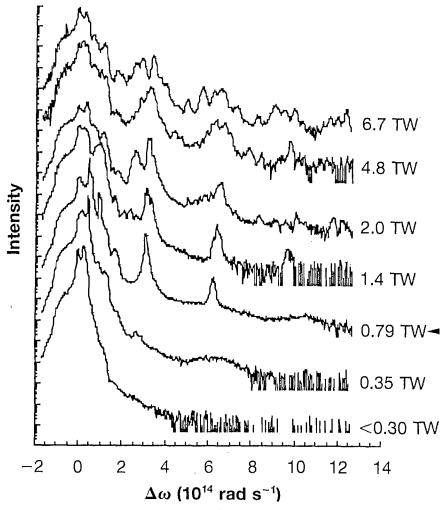

Fig. 2. Spectrum of RFS light as a function of laser power for fixed backing pressure (150 psi), corresponding to an electron density of 2.3×10^{19} cm^{-3} or n_e/n_c = 0.02. The curves are corrected for spectrometer-detector response and plotted on a logarithmic scale but offset from each other to prevent overlap. Arrowhead indicates P_c.

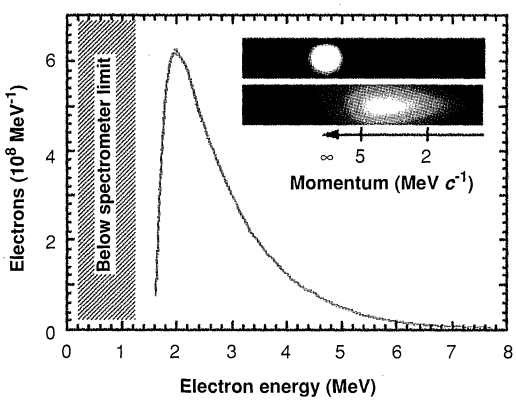

Fig. 3. The energy distribution of accelerated electrons measured with a magnetic spectrometer. The inset shows the collimated electron beam with a dipole magnetic field (lower) and without it (upper).

direction was obtained with a plastic scintillator coupled to a photomultiplier tube, which was placed in the beam path 50 cm from the laser focus. The electrons were coupled out of the vacuum chamber by a 250-μm-thick aluminum window. A clear change in the total number of relativistic electrons as a function of laser power (Fig. 4) was observed when $P/P_c = 1.5$; the number jumped from zero to $>10^3$, with just a 15% change in power. At the highest power, more than 10^9 electrons were accelerated, the highest number ever by a laser wake field. A similar threshold behavior was observed when the backing pressure was varied for a fixed power of 1.5 TW. As the backing pressure was increased, a threshold was observed at a value corresponding to a density of 1×10^{19} cm^{-3}. Saturation was observed above a value corresponding to 2×10^{19} cm^{-3}, which is further evidence for the importance of ionization defocusing.

In a previous experiment, also using He and a similar laser (but with $\tau = 0.8$ ps), wavebreaking of an RFS-driven EPW (*22*) was reported at a laser power of 25 TW. It was attributed to the trapping of electrons from the bulk thermal distribution. The signature for it was assumed to be a sudden broadening of Raman peaks and an increase in both the number of high-energy electrons in the tail of the distribution (greater than 20 MeV) and their maximum energy (up to 44 MeV). The onsets of both electron acceleration and significant broadening of the transmitted light were observed in our experiment (Figs. 2 and 4) at the same density but at a laser power level of only 2 TW. In our case, we assume the electrons that were trapped were from a high-energy component of the velocity distribution, possibly preheated by small-angle Raman side-scattering (*21*). For instance, for an EPW with $\tilde{n}/n_e = 10\%$, the minimum trapping velocity was calculated to be more than 700 keV. Broadening was observed (Fig. 2) at a much smaller power than that implied previously (*22*) and then increased gradually with increasing power. Relativistic self-phase modulation can broaden the spectrum because the sign of the change in γ, and thus of ω, reverses at the peak of the laser pulse.

Spatial profiles of the laser intensity at the laser beam waist (Fig. 5, A and B) were obtained at low laser intensity with an equivalent plane imaging system and a CCD camera readout. Spatial profiles of the electron beam (in vacuum, without a window between them) (Fig. 5, C and D) were produced with the laser spots shown in Fig. 5, A and B, respectively. These images show a naturally collimated beam of self-trapped electrons that were accelerated by a laser wake field. Previously, only either an externally accelerated beam was injected (*23*) or self-trapped electrons were collimated by an external aperture (*22*).

The electron beam spatial distribution at the film location is determined by a convolution between the spatial distribution of trapped electrons and the accelerating fields at the source. The accelerating fields, proportional to the EPW amplitude (and, ultimately, to the laser amplitude), give the electrons both radial and longitudinal momenta. Radial momenta can be acquired by several means: ponderomotive drift, side-scattering, and RFS from a diverging laser beam. We attribute their origin mostly to the last of these because the electron beam divergence appeared to follow that of the laser beam, and the electron energy distribution was independent of angle. The half-angle divergence of the outside of the beam, inferred from the beam size in Fig. 5C, is approximately 10°. This divergence angle, and an assumption that the electron source size is approximately the same as the laser spot size, can be used to estimate an electron beam emittance of 3.7 mm-mrad, which is the same as that of the laser. However, under certain circumstances, they both decrease by a factor of 3, as shown in Fig. 5D. This transverse emittance and number of electrons (>0.5 nC) are both comparable to state-of-the-art radio-frequency (RF) photoinjector linear accelerators.

The picture far from the source can be thought of as a micrograph, with a magnification given by the ratio of the size of the electron beam at the location of the film to the size of it at the source. Note the similarity in Fig. 5 between the laser spots and the electron beams that they produce. The far-field electron beam spatial distribution resembles the laser's near-field intensity distribution (at its focus) and, by inference, the EPW profile (as expected because the latter is proportional to the former). There can be a one-to-one correspondence as the radial momenta acquired by any of the above mechanisms should be exclusively outward from the laser axis. The hole in the center of the electron beam in Fig. 5D occurs only in the low-emittance regime. The hole apparently results from the lack of electrons on axis to be accelerated or, for that matter, to even constitute an EPW. Electron cavitation is just that: a dearth of electrons in the laser channel. In fact, a recent 3D PIC simulation—with similar laser parameters but higher plasma density (near critical)—predicts total evacuation of both electrons and ions on axis (*24*). Spatial imaging of the electron beam provides a

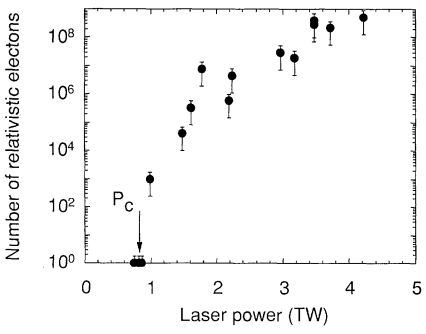

Fig. 4. The number of relativistic electrons as a function of incident laser power for a fixed backing pressure (150 psi), corresponding to an electron density of 2.3×10^{19} cm^{-3} or $n_e/n_c = 0.02$.

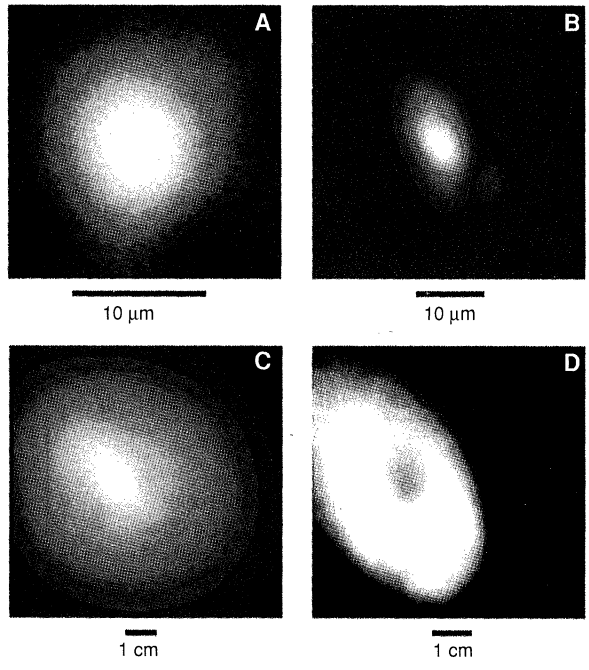

Fig. 5. (**A** and **B**) Images of the laser spot size at the beam waist, obtained with equivalent plane imaging and a CCD camera. In (A), the off-axis parabola produced a circular spot $2r = 17$ μm at $1/e^2$, which was used to obtain all of the previous figures. The image in (B) was obtained with a poorer quality parabola, producing an elliptical spot size measured to be $2r_x = 14$ μm and $2r_y = 22$ μm. (**C** and **D**) Images of the electron beam. The image in (C) corresponds to the laser focus shown in (A), with $P = 5.2$ TW. This laser focus was obtained with a scintillator screen and filtered with 25-μm-thick aluminum foil to prevent exposure by the laser light 15 cm from a jet of He gas. The image in (D) corresponds with the laser focus shown in (B), with $P = 2.8$ TW, obtained with use of photographic film (4000 ASA) 20 cm from a jet of Ar gas.

new diagnostic for the study of channel formation, which has relevance to any application requiring extended propagation of intense laser beams. Although these measurements are time-integrated, it is expected that the electrons are accelerated in microbunches that are a fraction of the plasma period (23 fs) in duration, separated by a plasma period, and in a macrobunch duration that is less than the laser pulse duration (400 fs).

REFERENCES AND NOTES

1. C. Max, J. Arons, A. B. Langdon, *Phys. Rev. Lett.* **33**, 209 (1974).
2. P. Mora and T. M. Antonsen Jr., *Phys. Rev. E* **53**, R2068 (1996).
3. G. Z. Sun, E. Ott, Y. C. Lee, P. Guzdar, *Phys. Fluids* **30**, 526 (1987).
4. A. B. Borisov *et al.*, *Phys. Rev. A* **45**, 5830 (1992).
5. D. C. Barnes, T. Kurki-Suonio, T. Tajima, *IEEE Trans. Plasma Phys.* **PS-15**, 154 (1987).
6. P. Maine *et al.*, *IEEE J. Quantum Electron.* **24**, 398 (1988); G. Mourou and D. Umstadter, *Phys. Fluids B* **4**, 2315 (1992).
7. T. Tajima and J. M. Dawson, *Phys. Rev. Lett.* **43**, 267 (1979).
8. P. Sprangle, E. Esarey, J. Krall, G. Joyce, *ibid.* **69**, 2200 (1992).
9. T. M. Antonsen Jr. and P. Mora, *ibid.*, p. 2204.
10. N. E. Andreev, L. M. Gorbunov, V. I. Kirsanov, A. Pogosova, R. R. Ramazashvili, *Pis'ma Zh. Eksp. Teor. Fiz.* **55**, 551 (1992) [*JETP Lett.* **55**, 571 (1992)].
11. J. Krall, A. Ting, E. Esarey, P. Sprangle, G. Joyce, *Phys. Rev. E* **48**, 2157 (1993).
12. E. Esarey, J. Krall, P. Sprangle, *Phys. Rev. Lett.* **72**, 2887 (1994).
13. C. Decker, W. B. Mori, T. Katsouleas, *Phys. Rev. E* **50**, R3338 (1994); W. B. Mori *et al.*, *Phys. Rev. Lett.* **72**, 1482 (1994).
14. S. V. Bulanov, F. Pegoraro, A. M. Pukhov, *Phys. Rev. Lett.* **74**, 710 (1995).
15. S. C. Wilks, W. L. Kruer, E. A. Williams, P. Amendt, D. C. Eder, *Phys. Plasmas* **2**, 274 (1995).
16. A. I. Akhiezer and R. V. Polovin, *Sov. Phys. JETP* **3**, 696 (1956).
17. C. A. Coverdale *et al.*, *Phys. Rev. Lett.* **74**, 4659 (1995).
18. A. J. Mackinnon *et al.*, *ibid.* **76**, 1473 (1996).
19. The EPW amplitude was estimated with the standard Bragg scattering equation, $P_s/P_0 \sim (\Delta n/n_e)^2(n_e/n_c)^2(V/2z_r\lambda^2)$, where V is the volume the plasma wave occupies [R. E. Slusher and C. M. Surko, *Phys. Fluids* **23**, 472 (1980)]. This result was consistent with a numerical simulation that simply allows a laser pulse to undergo a Fourier transform. This laser pulse is then phase-modulated by a copropagating plasma wave and oscillating background electrons such that $I(t) = I_0(t)\exp[-i(2\pi/\lambda)\Delta n(t)L]$, where $\Delta n(t) = -[\omega_{p0}^2/2\omega^2\gamma(t)][1 + (\tilde{n}/n_e)\cos W_p(t)t]$ is the change of refractive index and $I_0(t)$ is the initial laser pulse intensity.
20. Equation 3 predicts an amplitude of $\tilde{n}/n_e \sim 5$ to 40% (which corresponds to 9.4 to 11.6 e foldings) for 0.6 TW to 1 TW, assuming growth from an initial noise level predicted by theory (*21*), 4×10^{-6}, and a propagation distance $z/z_R = 1.0$, limited by refraction; the latter quantities have not actually been measured.
21. K.-C. Tzeng, W. B. Mori, C. D. Decker, *Phys. Rev. Lett.* **76**, 3332 (1996).
22. A. Modena *et al.*, *Nature* **377**, 606 (1995).
23. K. Nakajima *et al.*, *Phys. Rev. Lett.* **74**, 4428 (1995).
24. A. Pukhov and J. Meyer-ter-Vehn, *ibid.* **76**, 3975 (1996).

25. We would like to thank P. Bucksbaum, M. Downer, R. Gilgenbach, D. Gustafson, L. Jones, Y. Y. Lau, P. Le Blanc, X. Liu, and B. Roe for many useful discussions. Financial support was provided by the National Science Foundation and the U.S. Department of Energy.

2 February 1996; accepted 8 May 1996

Rates of DNA-Mediated Electron Transfer Between Metallointercalators

M. R. Arkin, E. D. A. Stemp, R. E. Holmlin, J. K. Barton,* A. Hörmann, E. J. C. Olson, P. F. Barbara*

Ultrafast emission and absorption spectroscopies were used to measure the kinetics of DNA-mediated electron transfer reactions between metal complexes intercalated into DNA. In the presence of rhodium(III) acceptor, a substantial fraction of photoexcited donor exhibits fast oxidative quenching (>3×10^{10} per second). Transient-absorption experiments indicate that, for a series of donors, the majority of back electron transfer is also very fast (~10^{10} per second). This rate is independent of the loading of acceptors on the helix, but is sensitive to sequence and π stacking. The cooperative binding of donor and acceptor is considered unlikely on the basis of structural models and DNA photocleavage studies of binding. These data show that the DNA double helix differs significantly from proteins as a bridge for electron transfer.

Many researchers have considered whether the aromatic heterocyclic bases in duplex DNA offer a medium for fast, long-range electron transfer (ET) (*1–10*). Intercalated electron donors and acceptors provide a direct probe of the DNA π stack. Subnanosecond luminescence quenching of photoexcited Ru(II) donors by Rh(III) acceptors occurs when both complexes are intercalatively stacked into B-form DNA (B-DNA), but fast quenching is not observed with a nonintercalating acceptor in a reaction with comparable driving force (*3*, *4*). Indeed, with metallointercalators covalently attached to a 15–base pair (bp) DNA duplex and separated by >40 Å, a lower limit on the intramolecular quenching was set at ~3×10^9 s^{-1} (*4*). Here we have used ultrafast emission and absorption spectroscopies to examine fast ET reactions mediated by DNA with a series of noncovalently bound, intercalated metal complexes.

The photoexcited donors (Fig. 1) display large enhancements of luminescence upon DNA intercalation (*11–13*). Two-dimensional nuclear magnetic resonance (NMR) studies show that the dppz ligand of $Ru(phen)_2dppz^{2+}$ (phen, 1,10-phenanthroline; dppz, dipyridophenazine) intercalates into B-DNA from the major groove (*14*) with a binding constant of >10^7 M^{-1} (*15*). For $M(phen)_2dppz^{2+}$ derivatives (M = Ru, Os), the lowest energy electronic transition is characterized by metal-to-ligand charge transfer (MLCT) directed onto the dppz ligand (*13*, *16*). In aqueous solutions, the excited state of these complexes is quenched by proton transfer from water to the phenazine N atoms (*12*, *13*); when the dppz ligand is protected from water by DNA intercalation, this pathway is inhibited, and emission typical of these polypyridyl complexes is detected. Hence, excitation of the complexes bound to DNA promotes an electron onto the intercalating ligand, directing it into the π stack.

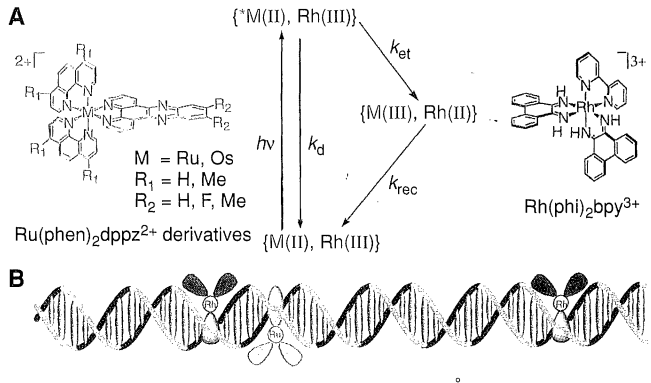

Fig. 1. (**A**) Intercalating donors (M = Ru, Os) and acceptor Rh(III) and the ET cycle. Photoexcitation of M(II) forms the excited state *M(II), which can radiatively decay (k_d) or can be quenched by ET with Rh(III) (k_{et}) to form M(III)-Rh(II) and then recombine (k_{rec}). Photoinduced ET may yield either $Rh(II)(phi)_2bpy$ or Rh(III)(phi)(phi^-)bpy, both symbolized as Rh(II). (**B**) Ru and Rh bound to DNA at typical ratios used in these experiments; the donor-acceptor distances shown correspond to 17 and 85 Å.

M. R. Arkin, E. D. A. Stemp, R. E. Holmlin, J. K. Barton, Beckman Institute, California Institute of Technology, Pasadena, CA 91125, USA.
A. Hörmann, E. J. C. Olson, P. F. Barbara, Department of Chemistry, University of Minnesota, Minneapolis, MN 55455, USA.
*To whom correspondence should be addressed.